Mechanically patterning the embryonic airway epithelium

Victor D. Varner[a], Jason P. Gleghorn[a], Erin Miller[b], Derek C. Radisky[b], and Celeste M. Nelson[a,c,1]

[a]Department of Chemical & Biological Engineering, Princeton University, Princeton, NJ 08544; [b]Department of Cancer Biology, Mayo Clinic Cancer Center, Jacksonville, FL 32224; and [c]Department of Molecular Biology, Princeton University, Princeton, NJ 08544

Edited by Kristi S. Anseth, Howard Hughes Medical Institute, University of Colorado Boulder, Boulder, CO, and approved June 10, 2015 (received for review February 27, 2015)

Collections of cells must be patterned spatially during embryonic development to generate the intricate architectures of mature tissues. In several cases, including the formation of the branched airways of the lung, reciprocal signaling between an epithelium and its surrounding mesenchyme helps generate these spatial patterns. Several molecular signals are thought to interact via reaction-diffusion kinetics to create distinct biochemical patterns, which act as molecular precursors to actual, physical patterns of biological structure and function. Here, however, we show that purely physical mechanisms can drive spatial patterning within embryonic epithelia. Specifically, we find that a growth-induced physical instability defines the relative locations of branches within the developing murine airway epithelium in the absence of mesenchyme. The dominant wavelength of this instability determines the branching pattern and is controlled by epithelial growth rates. These data suggest that physical mechanisms can create the biological patterns that underlie tissue morphogenesis in the embryo.

buckling | instability | mechanical stress | morphodynamics | morphogenesis

Space-filling, branched networks form the basic architecture of several organs, including the lung, kidney, and mammary gland. In the developing embryo, these complex structures originate as simple epithelial tubes. To form a ramified network, the initial tubular geometry is molded by a series of branching events, patterned in both space and time (1–3). In most cases, branching involves reciprocal signaling between adjacent tissues (4, 5), but it remains unclear how the locations of new branches are determined.

Airway branching is highly stereotyped in the developing mouse lung (6) and regulated in part by fibroblast growth factors (FGFs) (7). New epithelial branches are thought to emerge at locations adjacent to a prepattern of focal expression of FGF10 in the neighboring mesenchyme (8, 9) (Fig. 1*A*), a molecular mechanism with remarkable similarity to the induction of *Drosophila* tracheal branching by the FGF homolog Branchless (10). Moreover, the prepattern of FGF10 is regulated by reciprocal feedback between core signaling pathways, including those downstream of sonic hedgehog, bone morphogenetic protein, Wnt, and Notch (5, 11–13). These molecular signals are thought to interact via a reaction-diffusion mechanism (14, 15) to generate the spatial template of FGF10 (16) and are typically assumed to be sufficient to pattern branch locations along the airway epithelium (5, 10). This rich molecular description, however, overlooks the role that mechanical cues might play in establishing biological patterns. The pattern of villi in the developing gut, for instance, is determined by physical buckling (17, 18).

When the mesenchyme is removed, thus disrupting reciprocal signaling, isolated epithelia still branch in response to FGF1 or FGF10 (19, 20). In these culture models, the exogenous growth factors are present ubiquitously, with no apparent spatial pattern (Fig. 1*B*). In the absence of a mesenchymal prepattern of FGF, it is unclear how the epithelial branching pattern is specified. These data suggest the requirement for additional, nonchemically templated patterning mechanisms.

Results

Epithelial Branches Form Simultaneously with a Characteristic Wavelength. To determine the dynamics of mesenchyme-free branching, we performed time-lapse imaging analysis of epithelial explants and quantified the resulting kinematics. Mesenchyme was removed from embryonic day 12.5 mouse lungs, and isolated epithelia were embedded in 3D gels of reconstituted basement membrane protein (Matrigel) (Fig. 1*C*). Experiments using mice transgenic for GFP downstream of the vimentin gene promoter confirmed complete removal of the mesenchyme (Fig. S1). As the cultured epithelium grew and expanded, new branches formed simultaneously (Fig. 1*D* and Movie S1), casting the epithelium into a folded geometry with characteristic wavelength, λ, of ∼100 μm (Fig. 1 *E* and *F*). These branches then grew outward, extending further into the surrounding gel (Fig. 1*G*). During this process, the perimeter of the branching epithelium (Fig. 1 *F* and *G*) increased in time as the epithelium expanded (Fig. 1*H*).

Spatial Patterns of Proliferation Do Not Appear Until Branches Have Already Formed. The embryonic airway epithelium is highly proliferative in vivo (21), and it is often assumed that new branches result from localized growth (22). We therefore quantified 3D patterns of proliferation within mesenchyme-free explants (Fig. 2 *A* and *B*) and reconstructed the epithelial surface (Fig. 2*C*) using confocal images of immunofluorescence staining for E-cadherin (Movie S2). We then computed the mean curvature, κ, along this reconstructed surface and compared the distribution of mean curvature to that of cell proliferation (Fig. 2*D*). Mean curvature was highest in the distal tips of extending branches, coincident with elevated levels of proliferation (20, 23, 24) (Fig. 2*D*).

Significance

During branching morphogenesis of the developing lung, it is generally thought that a spatial template of biochemical cues determines the airway branching pattern. Here, however, we demonstrate that physical mechanisms can control the pattern of airway branching. Using a combination of 3D culture experiments and theoretical modeling, we show that a growth-induced physical instability initiates the formation of new epithelial branches. Tuning epithelial growth rate controls the dominant wavelength of the instability, and thereby the branching pattern. These findings emphasize the role of mechanical forces during morphogenesis and indicate that lung development is not a closed genetic system. Physical cues also regulate the spatially patterned cell behaviors that underlie organ assembly in the embryo.

Author contributions: V.D.V., J.P.G., and C.M.N. designed research; V.D.V. and J.P.G. performed research; E.M. and D.C.R. contributed new reagents/analytic tools; V.D.V. analyzed data; and V.D.V. and C.M.N. wrote the paper.

The authors declare no conflict of interest.

This article is a PNAS Direct Submission.

[1]To whom correspondence should be addressed. Email: celesten@princeton.edu.

This article contains supporting information online at www.pnas.org/lookup/suppl/doi:10.1073/pnas.1504102112/-/DCSupplemental.

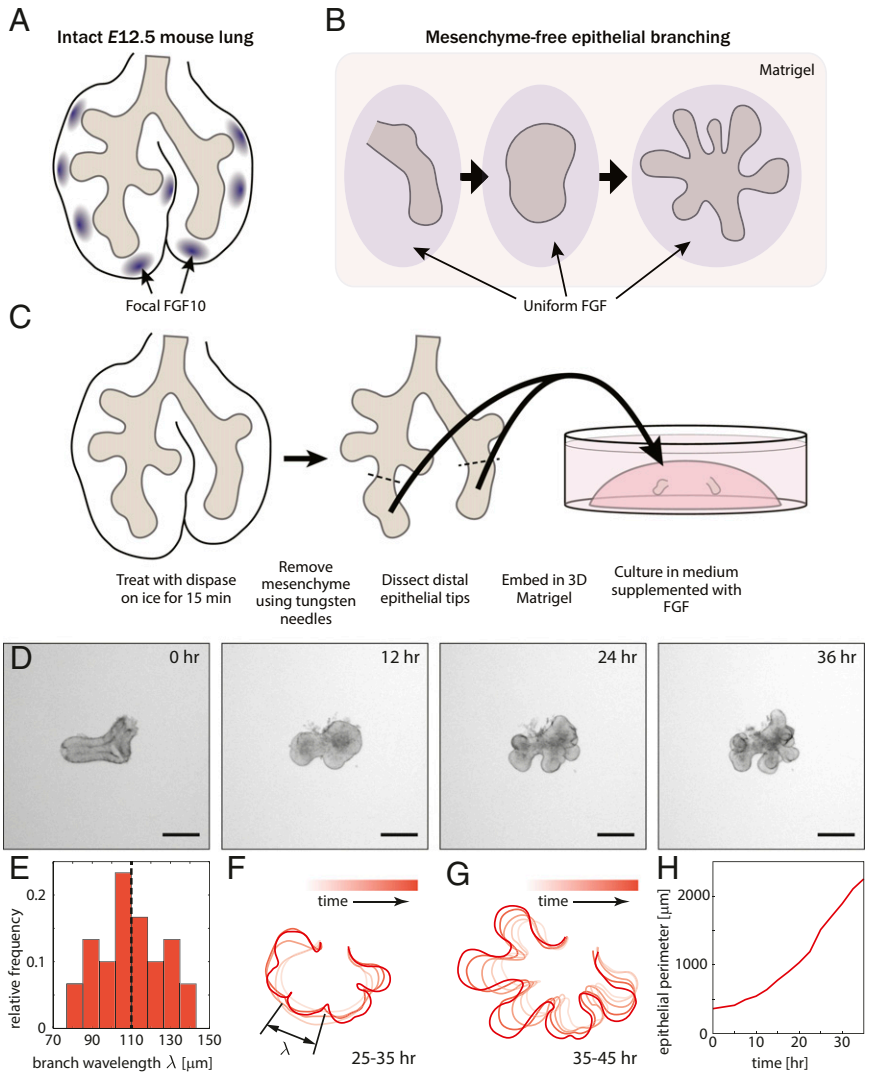

Fig. 1. Morphodynamics of mesenchyme-free branching. Schematic of FGF prepattern in (*A*) intact mouse lung and (*B*) during mesenchyme-free culture. (*C*) Schematic of mesenchyme-free culture assay. (*D*) Time-lapse bright-field images of mesenchyme-free epithelial branching. (Scale bars, 200 μm.) (*E*) Epithelial branches form simultaneously with characteristic wavelength λ. Traced contours of epithelium during (*F*) branch initiation and (*G*) branch elongation. (*H*) Epithelial perimeter over time for a representative explant.

We applied a similar analysis to mesenchyme-free epithelia before the initiation of branching (Fig. 2 *E*–*G*). In these explants, variations in surface curvature were more attenuated, and mean curvature and cell proliferation were not spatially correlated (Fig. 2*G*). These data indicate that distinct patterns of cell proliferation do not emerge until branches have already formed, consistent with previous findings (23).

Because new branches form simultaneously, and patterns of proliferation are relatively uniform before the onset of branching (Fig. 2*G*), we hypothesized that a growth-induced mechanical instability might drive the observed epithelial folding, similar to how a beam on an elastic foundation buckles under in-plane compressive loading (25). At a critical compressive load, the initially straight beam is no longer stable and spontaneously develops a buckled, wave-like morphology.

Modeling Constrained Epithelial Growth in an Elastic Gel. To test the plausibility of this hypothesis, we constructed a simple physical model for the proliferating airway epithelium supported by an elastic foundation (i.e., the surrounding gel) (Fig. 3*A*). As a first approximation, we ignored the effects of initial curvature and modeled the epithelium as an infinite flat layer (see *SI Text* for a more detailed description of the mathematical model). Epithelial proliferation was included by decomposing the overall mechanical strain in the layer (ϵ) into a component due to growth (ϵ_g) and a component due to elastic deformation (ϵ^*) using the relation $\epsilon = \epsilon^* + \epsilon_g$ (Fig. S2). [This superposition of strains is a linearized version of the more general theory for finite volumetric growth (26) and is valid for small deformations, a condition that, as a first approximation, was also assumed here.] We then incorporated this framework for biological growth into the classic equation for buckling of an elastic layer supported by an elastic half-space (27, 28). Here, the compressive in-plane force (N_g) was induced by constrained growth in the proliferating epithelium (i.e., for $\epsilon_g > 0$, N_g is compressive).

Because spatial patterns of proliferation were not observed before branching (Fig. 2 *E*–*G*), we considered the case of uniform growth in the epithelium, $\epsilon_g(x,y) = \epsilon_g^o$. In this case, the proliferating epithelium expands, reaches instability, and folds out-of-plane (Fig. 3*B*) with a dominant wavelength given by $\lambda_{cr_e} = 2\pi h \sqrt[3]{B/3B_f}$, where $B = E/(1-\nu^2)$ and $B_f = E_f/(1-\nu_f^2)$ represent elastic moduli for the epithelium and surrounding gel, respectively, and depend on the Young's modulus E and

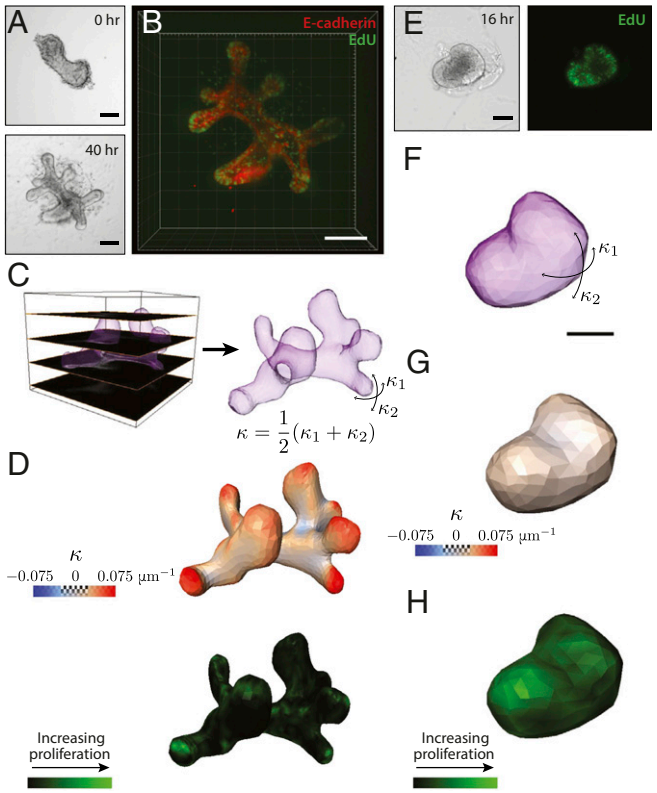

Fig. 2. Patterns of cell proliferation during mesenchyme-free branching. (*A*) Mesenchyme-free explant after 0 h and 40 h of culture. (Scale bars, 100 μm.) (*B*) Three-dimensional reconstruction of proliferation assessed via EdU incorporation (green). Airway epithelium colabeled by immunofluorescence staining for E-cadherin (red). (Scale bar, 200 μm.) (*C*) Three-dimensional surface reconstruction of characteristic epithelial geometry after branch initiation. (*D*) Plots of both mean curvature and EdU staining after branch initiation. (*E*) Mesenchyme-free explant after 16 h of culture (EdU, green). (Scale bar, 100 μm.) (*F*) Three-dimensional surface reconstruction of characteristic unbranched geometry. (Scale bar, 100 μm.) (*G* and *H*) Plots of both (*G*) mean curvature and (*H*) EdU staining before branch initiation.

Poisson's ratio ν of each material. Thus, for the case of an elastic instability, the dominant wavelength is controlled by the relative difference in stiffness between the two layers.

Experimentally Testing the Elastic Instability Hypothesis. The results of the elastic model suggested that uniform growth along the airway epithelium might be sufficient to produce branches of characteristic wavelength in the absence of a biochemical template, with the relative difference in stiffness between the epithelium and the gel specifying the locations of new branches. To test this mechanism experimentally, we cultured epithelial explants in different concentrations of Matrigel, thereby varying the mechanical properties of the gel (Fig. 3 *C–H*), which were measured using unconfined compression tests (*Methods* and Fig. S3). Based on the above relation for λ_{cr_e}, we would predict the dominant wavelength to decrease as gel stiffness increases. Indeed, we found that branch wavelengths varied as a function of gel concentration, with shorter wavelengths observed in explants cultured within higher concentrations of Matrigel (Fig. 3*I*). However, importantly, epithelial growth also depended on gel concentration: Epithelial contour perimeters increased more rapidly (Fig. 3*J*), branches formed at earlier time points (Fig. 3 *C–H*), and the rate of proliferation increased (Fig. S4) at higher concentrations of Matrigel.

In addition to extracellular matrix proteins, Matrigel also contains growth factors that can induce proliferation (29). To parse the relative roles of mechanics and proliferation, we used methylcellulose to alter the mechanical properties of Matrigel (Fig. 4*A*), while maintaining constant ligand density. Altering the stiffness of the gel (Fig. S5) did not significantly affect branch wavelengths (Fig. 4 *A–D*), suggesting that the mechanical properties of the foundation do not control branching and, therefore, that a purely elastic instability does not pattern the locations of new branches. The concentration-dependent differences in epithelial growth rates described above (Fig. 3*J*), however, suggested the possibility for time-dependent, viscoelastic effects.

Epithelial Branching Is Driven by a Growth-Induced, Viscoelastic Instability. Returning to our mathematical model (Fig. 3 *A* and *B*), we thus included the effects of viscoelasticity in our governing equations (see *SI Text* for a more detailed description of the model). As a first approximation, we considered the simplest case of an elastic epithelial layer supported by a Maxwell-type viscoelastic foundation. In this case, the dominant wavelength (Fig. 3*B*) was not predicted to depend on the mechanical properties of the foundation, and was instead given by the relation $\lambda_{cr_v} = \pi h \sqrt{B/N_{g_{cr}}}$, where B represents the elastic modulus of the epithelium and $N_{g_{cr}}$ represents the critical in-plane load, which depends linearly on the amount of growth, $\epsilon_{g_{cr}}$. This relation predicts shorter branch wavelengths at higher proliferation rates, consistent with those observed when varying the concentration of Matrigel (Fig. 3 *C–H*). Also, importantly, this mechanism is consistent with our methylcellulose experiments, which suggested that branch wavelengths are independent of the mechanical properties of the gel.

To further test this mechanism experimentally, we cultured explants in gels supplemented with different concentrations of FGF (Fig. 4 *E–H*) to modulate epithelial proliferation (Fig. S6) independently of the mechanical properties of the gel. Consistent with the predictions of our model, branch wavelengths decreased (Fig. 4*I*) and the rate of epithelial expansion increased at higher concentrations of FGF (Fig. 4*J*). The pattern of branching could thus be tuned by varying the epithelial growth rate.

We then extended our viscoelastic model to predict how these epithelial folds might emerge from the initially unpatterned tissue. Because, in actuality, no epithelium is perfectly flat, the geometry of the undeformed tissue was taken to consist of random, infinitesimally small deflections $[v_0(x)]$, which could then be decomposed into a Fourier series with different components at different spatial frequencies (Fig. 4*K*). In the model, these irregularities were sufficient to initiate a folding instability in the growing epithelial layer, and regular folds of characteristic wavelength emerged spontaneously from the noisy initial conditions. For different values of ϵ_g, the increase in amplitude (with time t) of each Fourier component within $v_0(x)$ depended upon how closely the wavelength of each corresponded to the dominant wavelength of the instability λ_{cr_v}. Those components with wavelengths nearest to λ_{cr_v} grew most quickly, and thus established the wave-like geometry of the epithelial layer (see *SI Text* for a more detailed description of the model). Our simulations predicted shorter branch wavelengths at increased values of ϵ_g, consistent with our experimental results (Fig. 4 *L* and *M*). The computed branch wavelengths were robust to variations in the initial irregularities in the epithelium. Taken together, these results indicate that a viscoelastic instability, driven by proliferation, defines the locations of epithelial branches in the absence of mesenchyme.

Discussion

Biological patterns are thought to arise primarily as a consequence of biochemical signaling. In several species, morphogens interact via reaction-diffusion kinetics to generate discrete patterns of gene expression in the embryo (14). Other (nonchemically mediated) mechanisms of pattern formation have received considerably less attention (30). Here, in the absence of any biochemical template,

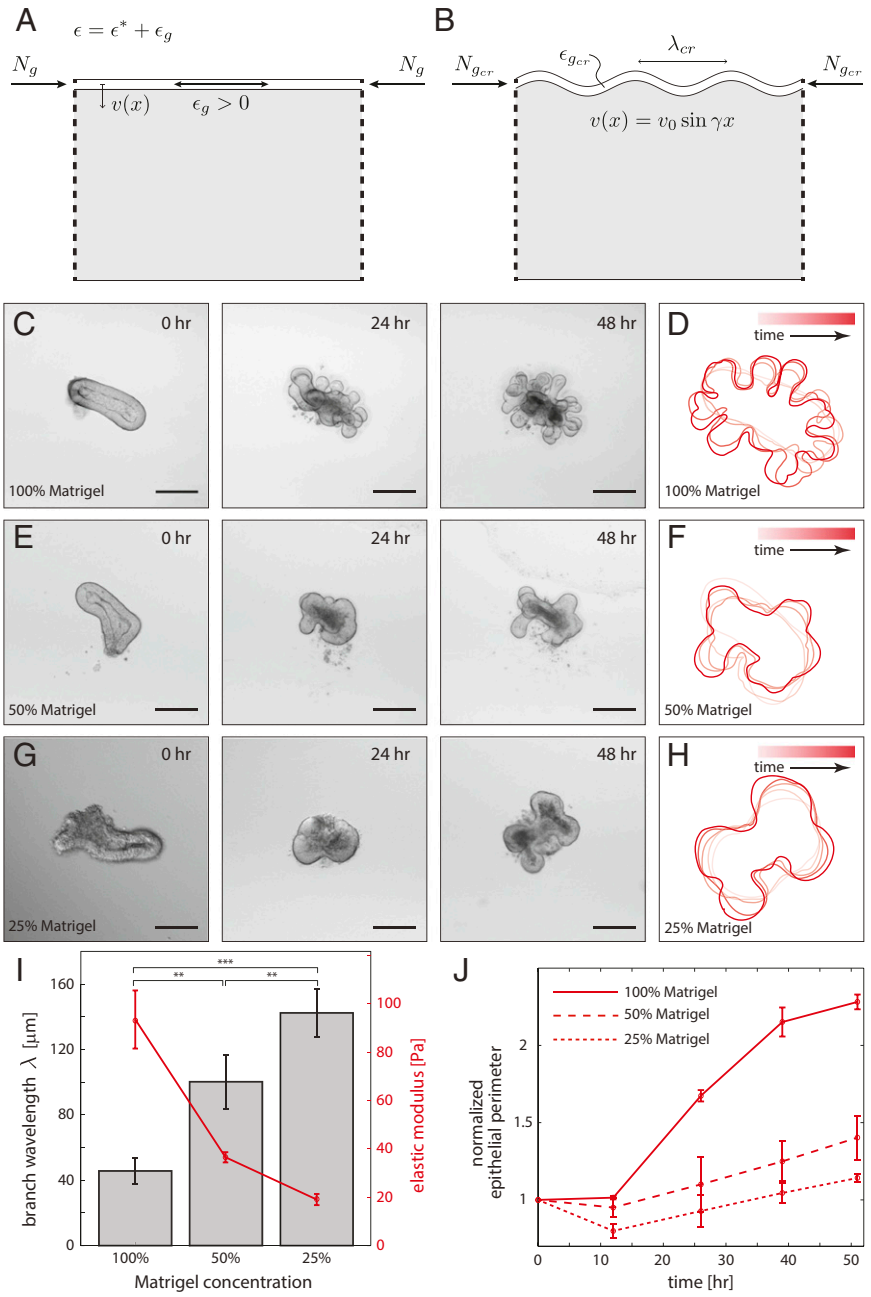

Fig. 3. Tuning branch wavelength. (*A* and *B*) Simple linear model for a growing infinite sheet supported by a viscoelastic foundation. (*C–H*) Tuning branch wavelength experimentally by varying the concentration of Matrigel in the surrounding gel. Traced epithelial contours reveal branching dynamics. (Scale bars, 200 μm.) (*I*) Branch wavelength as a function of gel concentration. Shown are mean ± SD for four experimental replicates. (*J*) Epithelial expansion during branch formation. Shown are mean ± SD for four experimental replicates. Statistics computed using one-way ANOVA with Tukey's post hoc test; $^{**}P < 0.01$; $^{***}P < 0.001$.

we have shown that purely physical interactions can drive biological patterning during branching morphogenesis of the embryonic airway epithelium. We took advantage of the mesenchyme-free culture system, which abolishes the prepattern of mesenchymal growth factors that are thought to coincide with locations of epithelial branches in the developing lung. Our data suggest that branches arise from a physical instability between the epithelium and its surrounding microenvironment. This folding is mediated by nonspatially patterned proliferation in the epithelium. Clear spatial patterns do not arise until branches have already formed, but it is unclear how the populations of highly proliferative cells, which are located at the tips of incipient branches, are either specified or maintained. The mechanical stresses induced by the initial folding of the epithelium may contribute to this spatial pattern, because mechanical stresses have been shown to control cell proliferation in 2D microfabricated tissues (31).

Importantly, mesenchyme-free branching is not unique to the developing lung. In the absence of mesenchyme, epithelial tissues from a variety of developing organs, including the salivary gland (32), kidney (33), and lacrimal gland (34), all generate similar branched structures when embedded in Matrigel. Even isolated fragments of intestinal epithelium produce similar geometries (35). Remarkably, in each case, proliferating cells are limited to the tips of the extending branches. Given the different tissue types, one would expect strikingly different biochemical microenvironments during morphogenesis, yet the topologies of

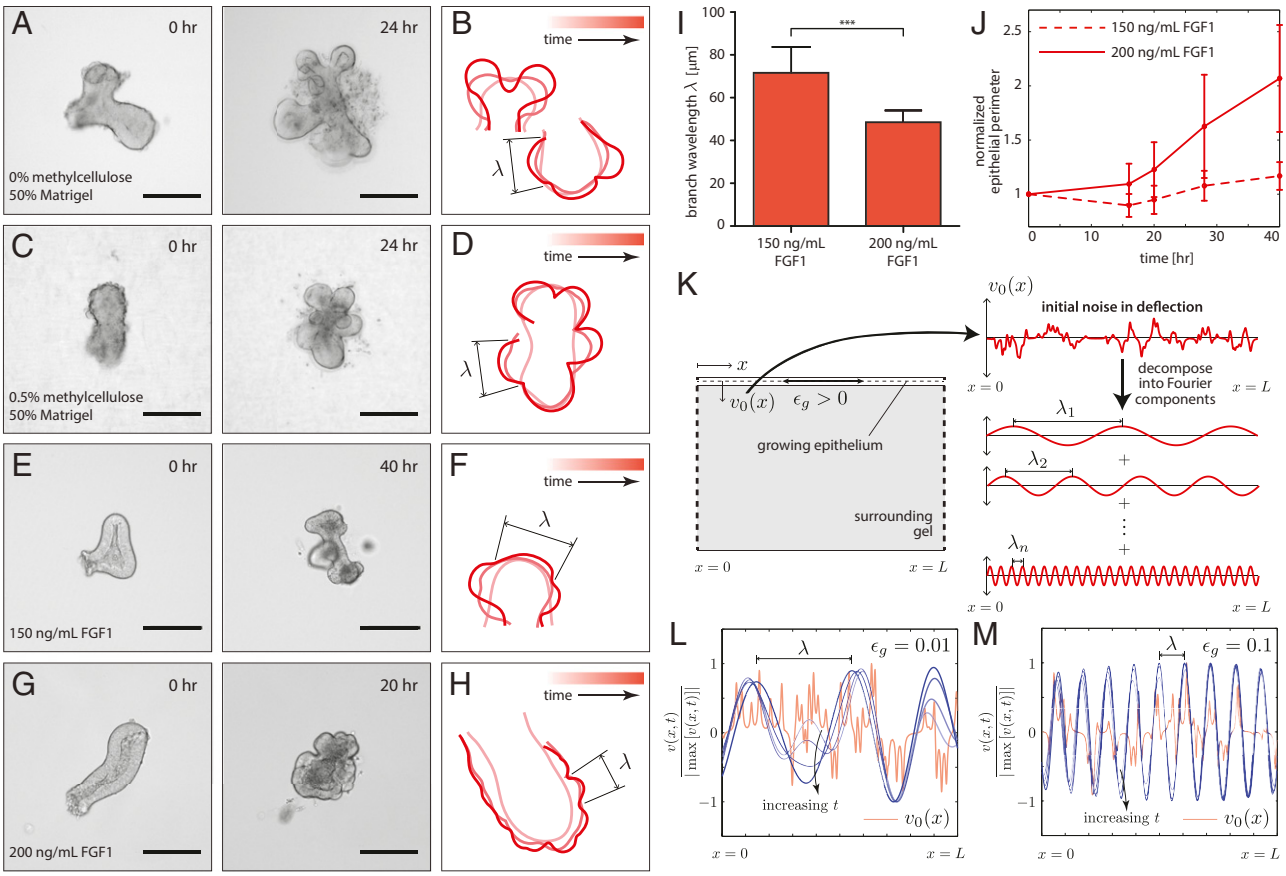

Fig. 4. Branch wavelengths are patterned by a growth-induced viscoelastic instability. (*A–D*) Varying the mechanical properties of the gel using methylcellulose. No differences in branch wavelength were observed between explants cultured in gels with methylcellulose (84 ± 8 μm) and those cultured in gels without (85 ± 9 μm). Data are mean ± SD for four experimental replicates. Statistics computed using Student's *t* test; $P = 0.82$. (*E–H*) Tuning epithelial proliferation using different concentrations of FGF in 100% Matrigel. Data are mean ± SD for four experimental replicates. (Scale bars, 200 μm.) (*I*) Branch wavelength as a function of FGF concentration. Statistics computed using Student's *t* test; $^{**}P < 0.01$. (*J*) Epithelial expansion over time at different concentrations of FGF. Data are mean ± SD for four experimental replicates. (*K*) Schematic for the viscoelastic time history of folding model. Noisy (infinitesimal) fluctuations in the initial geometry of the epithelial layer $v_0(x)$ are decomposed into Fourier components. As the epithelium grows, the amplitudes of those components, which correspond to the dominant wavelength of the instability, are preferentially amplified in time. (*L* and *M*) In our simulations, epithelial folds of characteristic wavelength λ emerge (with increasing time *t*) from the initial noise $v_0(x)$ (red curve). For increasing ϵ_g, we predict shorter branch wavelengths, as observed experimentally.

the branched architectures are similar. It is possible that a conserved physical mechanism underlies the folding of each of these epithelial tissues.

It is unclear whether a similar instability drives epithelial branching in the intact lung. Smooth muscle differentiation has been shown to increase the stiffness of mesenchymal tissues (18), so it is possible that the spatial patterns of airway smooth muscle might constrain a growth-induced instability within the epithelium in vivo. Alternatively, localized differences in proliferation between the epithelium and smooth muscle might pattern epithelial buckling. In both cases, contractile forces generated by mesenchymal cells might also influence the mechanics of epithelial branching (36, 37).

Regardless, our data diverge from the generally accepted view that airway branching is driven by differential epithelial proliferation. Here, we found the opposite. Patterned proliferation does not induce branching, but is a consequence of the epithelial folding that takes place as new branches form. In a sense, proliferation is "downstream" of branch initiation (22). Together, these data suggest that physical mechanisms are sufficient to pattern the morphogenesis of developing epithelia—a result that strongly asserts that material properties and mechanical cues, in addition to the well-recognized role of biochemical signals, need to be considered in studies of tissue development (38–40).

It remains unclear exactly how epithelial cells might respond to physical cues in their surrounding microenvironment. Here, we show that cells in the developing airway epithelium are insensitive to changes in the elastic properties of the surrounding matrix. They may, however, be responsive to other physical properties in the microenvironment (e.g., plasticity, material inhomogeneity, etc.). Additional work using sophisticated cogels of Matrigel and other synthetic or naturally derived matrices, with tunable mechanical properties (41), will be necessary to more fully elucidate the mechanoregulatory mechanisms at work during epithelial morphogenesis. Ultimately, these problems will demand interdisciplinary collaborations between engineers, physicists, materials scientists, and cell and developmental biologists and will require new experimental (42) and computational (43) approaches to quantify the mechanical forces and material properties that shape developing tissues.

Methods

Mesenchyme-Free Culture. Embryos were harvested from timed-pregnant CD1 (Charles River Laboratories) or vim-GFP (Mutant Mouse Regional Resource Center) mice at embryonic day 12–13, following protocols approved by the Princeton University Institutional Animal Care and Use Committee. Whole lung explants were dissected in ice-cold PBS using fine forceps. To isolate the airway epithelium, explants were incubated in 10 U/mL dispase (Invitrogen) on ice for 15 min; mesenchyme was then removed using fine tungsten needles (44).

Isolated epithelial explants were embedded in undiluted growth factor-reduced Matrigel (BD Biosciences), Matrigel diluted in culture medium (DMEM/F12 supplemented with 0.5% FBS, penicillin, and streptomycin), or in gels consisting of 50% Matrigel and 0.5% methylcellulose (Sigma; average molecular weight ~40,000). Gels were incubated at 37 °C for 30–60 min to set. Culture medium supplemented with FGF1 was then added, and explants were cultured for 48–72 h. Time-lapse movies were collected using a Nikon Ti-U inverted microscope customized with a spinning disk (BD Biosciences).

Quantifying Cell Proliferation. Proliferating cells were detected using the Click-iT EdU Imaging Kit (Invitrogen). Briefly, mesenchyme-free explants were pulsed with 5-ethynyl-2′-deoxyuridine (EdU) for 1 h, then fixed with 4% (wt/vol) paraformaldehyde in PBS and washed with 0.3% Triton-X-100 in PBS. Fixed explants were then incubated with primary antibody against E-cadherin and, subsequently, AlexaFluor-conjugated secondary antibodies to simultaneously label the airway epithelium. Explants were then removed from the surrounding gel, and confocal stacks were captured. Three-dimensional reconstructions of the airway epithelium and proliferating cells were generated using Imaris (Bitplane). From the confocal stacks of E-cadherin, we used Amira (FEI Visualization Sciences Group) to create surface reconstructions of the airway epithelium. The surface mean curvature κ was computed by $\kappa = (\kappa_1 + \kappa_2)/2$, where κ_1 and κ_2 are the principal curvatures. Cell proliferation was then mapped onto this reconstructed surface. Explants costained for EdU and Hoechst 33258 were used to quantify epithelial proliferation frequencies (Figs. S4 and S6).

Mechanical Testing. We performed unconfined compression tests of cylindrical gel specimens to estimate the mechanical properties of Matrigel (Figs. S3 and S5). Before gelation, fluorescent microspheres (500 nm in diameter) were suspended in the liquid Matrigel at 4 °C. This solution was injected into a cylindrical PDMS mold of defined diameter, which was conformally sealed to the underlying tissue culture polystyrene, and incubated at 37 °C for 30 min. The PDMS mold was removed, and confocal stacks of the cylindrical gel were captured before loading. A 12-mm-diameter glass coverslip of known weight was then used to mechanically compress the gel, and a subsequent confocal stack of the compressed configuration was captured within 1–2 min of loading. As a first approximation, the observed change in thickness was used to estimate the (linear) elastic modulus of the gel.

Theoretical Model. A detailed description of the model can be found in *SI Text*. The time history of folding simulations was solved using MATLAB.

ACKNOWLEDGMENTS. We thank Joe Tien for helpful discussions. This work was supported in part by NIH Grants GM083997, HL110335, HL118532, and HL120142; National Science Foundation Grant CMMI-1435853; the David and Lucile Packard Foundation; the Alfred P. Sloan Foundation; and the Camille & Henry Dreyfus Foundation. C.M.N. holds a Career Award at the Scientific Interface from the Burroughs Wellcome Fund.

1. Davies JA (2002) Do different branching epithelia use a conserved developmental mechanism? *BioEssays* 24(10):937–948.
2. Lu P, Werb Z (2008) Patterning mechanisms of branched organs. *Science* 322(5907): 1506–1509.
3. Affolter M, Zeller R, Caussinus E (2009) Tissue remodelling through branching morphogenesis. *Nat Rev Mol Cell Biol* 10(12):831–842.
4. Shannon JM, Hyatt BA (2004) Epithelial-mesenchymal interactions in the developing lung. *Annu Rev Physiol* 66:625–645.
5. Morrisey EE, Hogan BL (2010) Preparing for the first breath: Genetic and cellular mechanisms in lung development. *Dev Cell* 18(1):8–23.
6. Metzger RJ, Klein OD, Martin GR, Krasnow MA (2008) The branching programme of mouse lung development. *Nature* 453(7196):745–750.
7. Lebeche D, Malpel S, Cardoso WV (1999) Fibroblast growth factor interactions in the developing lung. *Mech Dev* 86(1–2):125–136.
8. Bellusci S, Grindley J, Emoto H, Itoh N, Hogan BL (1997) Fibroblast growth factor 10 (FGF10) and branching morphogenesis in the embryonic mouse lung. *Development* 124(23):4867–4878.
9. Park WY, Miranda B, Lebeche D, Hashimoto G, Cardoso WV (1998) FGF-10 is a chemotactic factor for distal epithelial buds during lung development. *Dev Biol* 201(2): 125–134.
10. Metzger RJ, Krasnow MA (1999) Genetic control of branching morphogenesis. *Science* 284(5420):1635–1639.
11. Warburton D, et al. (2000) The molecular basis of lung morphogenesis. *Mech Dev* 92(1):55–81.
12. Cardoso WV, Lü J (2006) Regulation of early lung morphogenesis: Questions, facts and controversies. *Development* 133(9):1611–1624.
13. Ornitz DM, Yin Y (2012) Signaling networks regulating development of the lower respiratory tract. *Cold Spring Harb Perspect Biol* 4(5):a008318.
14. Murray JD (2002) *Mathematical Biology* (Springer, New York), 3rd Ed.
15. Turing AM (1952) The chemical basis of morphogenesis. *Phil. Trans. R. Soc. B* 237(641): 37–72.
16. Menshykau D, Kraemer C, Iber D (2012) Branch mode selection during early lung development. *PLOS Comput Biol* 8(2):e1002377.
17. Hannezo E, Prost J, Joanny JF (2011) Instabilities of monolayered epithelia: Shape and structure of villi and crypts. *Phys Rev Lett* 107(7):078104.
18. Shyer AE, et al. (2013) Villification: How the gut gets its villi. *Science* 342(6155): 212–218.
19. Nogawa H, Ito T (1995) Branching morphogenesis of embryonic mouse lung epithelium in mesenchyme-free culture. *Development* 121(4):1015–1022.
20. Cardoso WV, Itoh A, Nogawa H, Mason I, Brody JS (1997) FGF-1 and FGF-7 induce distinct patterns of growth and differentiation in embryonic lung epithelium. *Dev Dyn* 208(3):398–405.
21. Wessells NK (1970) Mammalian lung development: Interactions in formation and morphogenesis of tracheal buds. *J Exp Zool* 175(4):455–466.
22. Varner VD, Nelson CM (2014) Cellular and physical mechanisms of branching morphogenesis. *Development* 141(14):2750–2759.
23. Nogawa H, Morita K, Cardoso WV (1998) Bud formation precedes the appearance of differential cell proliferation during branching morphogenesis of mouse lung epithelium in vitro. *Dev Dyn* 213(2):228–235.
24. Weaver M, Dunn NR, Hogan BL (2000) Bmp4 and Fgf10 play opposing roles during lung bud morphogenesis. *Development* 127(12):2695–2704.
25. Timoshenko S (1961) *Theory of Elastic Stability* (McGraw-Hill, New York), 2nd Ed.
26. Taber LA (2009) Towards a unified theory for morphomechanics. *Phil Trans R Soc A* 367(1902):3555–3583.
27. Biot MA (1937) Bending of an infinite beam on an elastic foundation. *J Appl Mech* 4:A1–A7.
28. Biot MA (1957) Folding instability of a layered viscoelastic medium under compression. *Proc R Soc Lond A Math Phys Sci* 242(1231):444–454.
29. Vukicevic S, et al. (1992) Identification of multiple active growth factors in basement membrane Matrigel suggests caution in interpretation of cellular activity related to extracellular matrix components. *Exp Cell Res* 202(1):1–8.
30. Taber LA (2000) Pattern formation in a nonlinear membrane model for epithelial morphogenesis. *Acta Biotheor* 48(1):47–63.
31. Nelson CM, et al. (2005) Emergent patterns of growth controlled by multicellular form and mechanics. *Proc Natl Acad Sci USA* 102(33):11594–11599.
32. Nogawa H, Takahashi Y (1991) Substitution for mesenchyme by basement-membrane-like substratum and epidermal growth factor in inducing branching morphogenesis of mouse salivary epithelium. *Development* 112(3):855–861.
33. Qiao J, Sakurai H, Nigam SK (1999) Branching morphogenesis independent of mesenchymal-epithelial contact in the developing kidney. *Proc Natl Acad Sci USA* 96(13): 7330–7335.
34. Makarenkova HP, et al. (2009) Differential interactions of FGFs with heparan sulfate control gradient formation and branching morphogenesis. *Sci Signal* 2(88):ra55.
35. Sato T, et al. (2009) Single Lgr5 stem cells build crypt-villus structures in vitro without a mesenchymal niche. *Nature* 459(7244):262–265.
36. Nogawa H, Nakanishi Y (1987) Mechanical aspects of the mesenchymal influence on epithelial branching morphogenesis of mouse salivary gland. *Development* 101(3): 491–500.
37. Wan X, Li Z, Lubkin SR (2008) Mechanics of mesenchymal contribution to clefting force in branching morphogenesis. *Biomech Model Mechanobiol* 7(5):417–426.
38. Miller CJ, Davidson LA (2013) The interplay between cell signalling and mechanics in developmental processes. *Nat Rev Genet* 14(10):733–744.
39. Taber LA (2014) Morphomechanics: Transforming tubes into organs. *Curr Opin Genet Dev* 27:7–13.
40. Varner VD, Nelson CM (2013) Let's push things forward: Disruptive technologies and the mechanics of tissue assembly. *Integr Biol (Camb)* 5(9):1162–1173.
41. Chaudhuri O, et al. (2014) Extracellular matrix stiffness and composition jointly regulate the induction of malignant phenotypes in mammary epithelium. *Nat Mater* 13(10):970–978.
42. Campàs O, et al. (2014) Quantifying cell-generated mechanical forces within living embryonic tissues. *Nat Methods* 11(2):183–189.
43. Wyczalkowski MA, Chen Z, Filas BA, Varner VD, Taber LA (2012) Computational models for mechanics of morphogenesis. *Birth Defects Res C Embryo Today* 96(2):132–152.
44. Del Moral PM, Warburton D (2010) Explant culture of mouse embryonic whole lung, isolated epithelium, or mesenchyme under chemically defined conditions as a system to evaluate the molecular mechanism of branching morphogenesis and cellular differentiation. *Methods Mol Biol* 633:71–79.
45. Biot MA (1954) Theory of stress-strain relations in anisotropic viscoelasticity and relaxation phenomena. *J Appl Phys* 25(11):1385–1391.
46. Flügge W (1975) *Viscoelasticity* (Springer-Verlag, Berlin), 2nd Ed.
47. Biot MA (1961) Theory of folding of stratified viscoelastic media and its implications in tectonics and orogenesis. *Geol Soc Am Bull* 72(11):1595–1620.
48. Biot MA, Odé H, Roever WL (1961) Experimental verification of the theory of folding of stratified viscoelastic media. *Geol Soc Am Bull* 72(11):1621–1631.
49. Reed J, Walczak WJ, Petzold ON, Gimzewski JK (2009) In situ mechanical interferometry of matrigel films. *Langmuir* 25(1):36–39.
50. Zaman MH, et al. (2006) Migration of tumor cells in 3D matrices is governed by matrix stiffness along with cell-matrix adhesion and proteolysis. *Proc Natl Acad Sci USA* 103(29):10889–10894.